

## ORIGINAL ARTICLE

# The SET domain protein PsKMT3 regulates histone H3K36 trimethylation and modulates effector gene expression in the soybean pathogen *Phytophthora sojae*

Han Chen  | Yujie Fang | Wenrui Song | Haidong Shu | Xi Li | Wenwu Ye  |  
Yuanchao Wang  | Suomeng Dong 

Department of Plant Pathology, the Key Laboratory of Integrated Management of Crop Diseases and Pests, Ministry of Education, the Key Laboratory of Plant Immunity, Nanjing Agricultural University, Nanjing, China

**Correspondence**

Suomeng Dong, Department of Plant Pathology, the Key Laboratory of Integrated Management of Crop Diseases and Pests, Ministry of Education, the Key Laboratory of Plant Immunity, Nanjing Agricultural University, Nanjing 210095, China.

Email: [smdong@njau.edu.cn](mailto:smdong@njau.edu.cn)

**Funding information**

National Key Research and Development Program of China, Grant/Award Number: 2022YFC2601000; National Natural Science Foundation of China, Grant/Award Number: 32100158 and 31721004; China Postdoctoral Science Foundation, Grant/Award Number: 2020M681641; Fundamental Research Funds for the Central Universities, Grant/Award Number: KYQN2022059

[Correction added on 14 February 2023, after first online publication: the Funding section has been updated in this version.]

**Abstract**

Plant pathogens secrete effector proteins to overcome host immunity and promote colonization. In oomycete plant pathogens, the expression of many effector genes is altered upon infection; however, the regulatory mechanisms are unclear. In this study, we identified a *su(var)3-9*, enhancer of zeste, and trithorax (SET) domain protein-encoding gene, *PsKMT3*, that was highly induced at early infection stages in *Phytophthora sojae*. Deletion of *PsKMT3* led to asexual development and pathogenicity defects. Chromatin immunoprecipitation followed by sequencing (ChIP-seq) and western blot analyses demonstrated that histone H3K36 trimethylation (H3K36me3) was significantly reduced genome-wide in mutants. RNA-seq analysis identified 374 genes encoding secreted proteins that were differentially expressed in *pskmt3* at the mycelium stage. The significantly altered genes encompassed the RxLR (Arg-Lys-Arg) effector gene family, including the essential effector genes *Avh23*, *Avh181*, *Avh240*, and *Avh241*. Transcriptome analysis at early infection stages showed misregulation of effector gene expression waves in *pskmt3*. H3K36me3 was directly and indirectly associated with RxLR effector gene activation. Our results reveal a role of a SET domain protein in regulating effector gene expression and modulating histone methylation in *P. sojae*.

**KEYWORDS**

effector gene expression, histone methylation, *Phytophthora*, SET domain protein, transcriptional regulation

## 1 | INTRODUCTION

Pathogen effector proteins are necessary for colonization and infection of hosts (Bialas et al., 2018; Jones & Dangl, 2006; Ngou et al., 2022; Sánchez-Vallet, 2018; Wang & Wang, 2018). Although plant pathogens—which include oomycetes, fungi, bacteria,

nematodes, and insects—have various lifestyles, most effector genes are induced upon infection (Chen et al., 2021; Petre et al., 2020; Ye et al., 2011). Studies on effector gene regulation and function enhance our understanding of pathogen virulence and host susceptibility (Jiang & Tyler, 2012; Wang & Wang, 2018). *Phytophthora sojae* is the causal agent of soilborne root and stem rot in soybean,

This is an open access article under the terms of the [Creative Commons Attribution-NonCommercial-NoDerivs](https://creativecommons.org/licenses/by-nc-nd/4.0/) License, which permits use and distribution in any medium, provided the original work is properly cited, the use is non-commercial and no modifications or adaptations are made.

© 2023 The Authors. *Molecular Plant Pathology* published by British Society for Plant Pathology and John Wiley & Sons Ltd.

which causes significant yield loss and costs \$1–2 billion annually (Tyler, 2007; Wrather & Koenning, 2006). *P. sojae* contains more than 2000 genes encoding secreted proteins, including RxLR effectors (Tyler, 2007). Most RxLR genes are induced 2- to 120-fold during early infection stages. These effectors are categorized into immediate-early and early effectors based on their expression pattern (Wang et al., 2011). As a consequence of their virulence function, misexpression of key effectors severely reduces the virulence of *P. sojae* transformants (Wang et al., 2011). However, how effector gene expression is concertedly regulated is unclear.

Histone modifications, which occur on a series of histone residues, play important roles in gene expression regulation and development in eukaryotes. Typically, trimethylation of histone H3 lysine 4 (H3K4me3) and lysine 36 (H3K36me3) are associated with actively expressed genes in euchromatic regions, whereas trimethylation of H3K9me and H3K27me are associated with gene repression in heterochromatin (Hyun et al., 2017; Rando & Chang, 2009; Wagner & Carpenter, 2012). However, H3K36me3 is not associated with gene activation in fungi (Janevska et al., 2018; Lukito et al., 2020). Furthermore, transcriptional repression by H3K36me3 has been reported in yeasts (Landry et al., 2003; Rechtsteiner et al., 2010; Strahl et al., 2002). Numerous cellular processes, such as DNA repair and alternative splicing, depend on H3K36me3 in higher eukaryotes (Kim et al., 2011; Sun et al., 2020). Histone methylation is modulated by methyltransferases and demethylases, and most specific histone lysine methyltransferases are SET domain-containing proteins (Dillon et al., 2005). KMT3 enzymes catalyse the methylation of H3K36 (Allis et al., 2007; Freitag, 2017; Wagner & Carpenter, 2012). The Set2–Rpb1 interacting (SRI) domain of the H3K36 methyltransferase Set2/KMT3 enables its interaction with RNA polymerase II and the methylation of H3K36 during transcriptional elongation (Hyun et al., 2017; Kizer et al., 2005). However, the function of H3K36me3 in oomycetes is unknown.

Histone methylation is involved in effector gene regulation in plant pathogens (Chujo & Scott, 2014; Clairet et al., 2021; Collemare & Seidl, 2019; Kramer et al., 2022; Meile et al., 2020; Soyer et al., 2014). Effector genes are repressed in vitro by heterochromatin marks, and the dynamics of histone modifications contribute to effector gene regulation (Meile et al., 2020; Soyer et al., 2014; Zhang et al., 2021). H3K36me3 can negatively or positively regulate effector gene expression in *Epichloë festucae* (Lukito et al., 2020). An effector gene in *P. sojae* is a target of heterochromatin marks (Wang et al., 2020). *P. sojae Avr1b* silencing mediated by H3K27me3 provides highly adaptive plasticity to overcome defence mechanisms in hosts carrying the corresponding R gene (Wang et al., 2020). Although the function of silencing histone marks in *P. sojae* epidemics has been evaluated, little is known about the role of active epigenetic marks, such as H3K36me3, in effector gene expression, and it remains to be elucidated to what degree these active marks affect pathogenicity and effector gene expression waves.

To investigate the mechanism of effector gene regulation in *P. sojae*, we characterized the gene encoding the SET domain protein

PsKMT3, which regulates histone H3K36 trimethylation. We found that PsKMT3 is involved in pathogenicity regulation and asexual development. Genes encoding secreted proteins were enriched among differentially expressed genes (DEGs), and transcriptomic analysis showed dysregulation of the expression of effector gene waves in *pskmt3*. Moreover, PsKMT3-dependent H3K36me3 is important in effector gene regulation at the mycelium stage and is involved in inducing RxLR gene expression during infection. Our findings suggest an effector gene regulation mechanism in *P. sojae*, which will facilitate the development of novel fungicides and disease management strategies.

## 2 | RESULTS

### 2.1 | Identification of KMT3 proteins in oomycetes

H3K36 methylation is catalysed by the SET domain-containing KMT3 lysine methyltransferases, named according to the standard nomenclature for chromatin-modifying enzymes (Allis et al., 2007). To identify KMT3 proteins in oomycetes, we performed a Blastp search using KMT3 from *Saccharomyces cerevisiae* (ScSET2/NP\_012367.2) and *Neurospora crassa* (NcSET2/XP\_957740.1) as queries against 10 oomycete species of *Albugo*, Saprolegniaceae, Pythiaceae, and Peronosporaceae. We identified three oomycete KMT3 clades with e-values  $<10^{-20}$ , and phylogenetic analysis revealed that PsKMT3 (Ps\_130312) was closely related to the queries NcSET2 and ScSET2 (Figure S1a). However, no *Albugo laibachii* or *Albugo candida* homologue clustered in clade 1. Clade 2a contained species of Pythiaceae and Peronosporaceae, suggesting KMT3 family duplication or loss events in oomycetes. Visualization of protein domains in clade 1 showed that they share the typical KMT3 domain organization: a combination of associated with SET (AWS) and SET domains (Figures 1a and S1b). Plant homeodomain (PHD) family proteins, which have been implicated in epigenetics and chromatin-mediated transcriptional regulation, were also identified (Sanchez & Zhou, 2011; Shi et al., 2007). Therefore, PsKMT3 could be involved in H3K36 methylation.

### 2.2 | Asexual development and pathogenicity were impaired in *pskmt3* mutants

PsKMT3 is induced at early infection stages (Ye et al., 2011) (Figure S2), suggesting that it regulates pathogenicity. To assess the biological role of PsKMT3, we generated three individual mutants by CRISPR/Cas9-mediated genome editing (Figures 1a–c and S3). Mutation of transformants T24 (–8 bp) and T89 (–5 bp) led to premature termination, and mutation of T99 (–1 bp) disrupted the reading frame (Figures 1b,c and S3). To determine whether PsKMT3 is involved in *P. sojae* development, we evaluated its effects on growth, sporulation, and zoospore production phenotypes. The growth rate of the three mutants showed 10% reduction compared with the

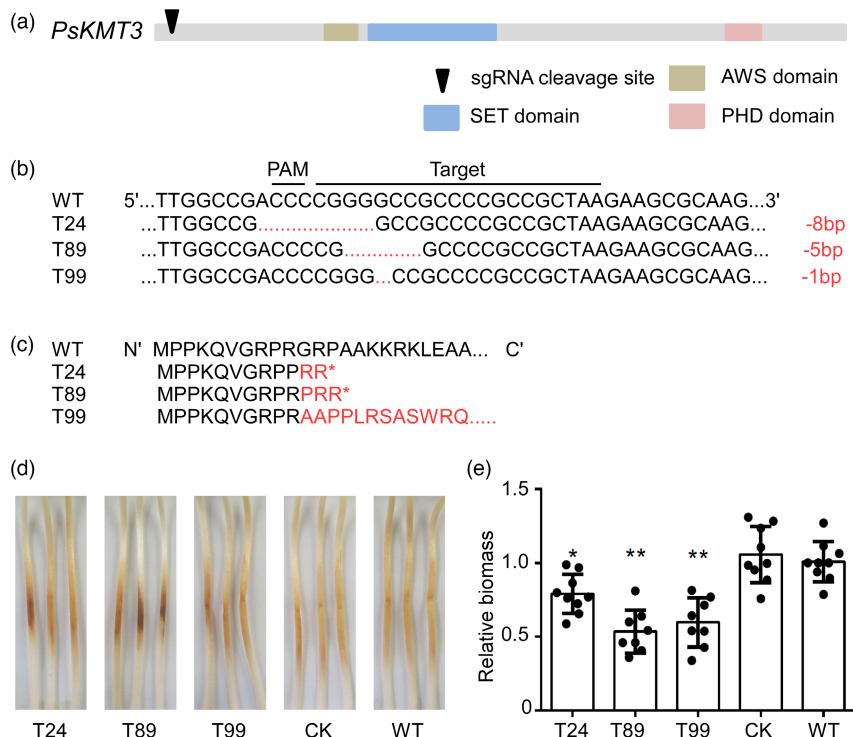


**FIGURE 1** Reduced pathogenicity of the *pskmt3* mutants. (a) Domain organization of *PsKMT3*. Black triangle, sgRNA cleavage site; squares, domains predicted by NCBI Conserved Domains using default parameters. (b,c) Nucleotide and amino acid sequences of *pskmt3* mutants compared with the wild type (WT). Red letters in (b) indicate the mutation type, and those in (c) indicate amino acid sequence differences compared with the WT. (d) Lesions on hypocotyls in soybean cultivar Hefeng47 incubated with three *PsKMT3* knockout mutants (T24, T89, T99), unedited strain CK, and WT at 48 h postinoculation (hpi). (e) Relative *Phytophthora sojae* biomass at 48 hpi in samples from (d) as determined by quantitative PCR analysis (WT-infected biomass was set to 1). x-axis, three *pskmt3* knockout mutants (T24, T89, and T99), control (CK), and WT; y-axis, relative biomass (ratio of the amounts of *P. sojae* DNA to soybean DNA). Asterisks indicate a significant difference according to one-way analysis of variance (\*\* $p < 0.01$ , \* $p < 0.05$ ). Experiments were performed in triplicate.

wild type (WT) and the unedited control strain (CK) on V8 medium (Figure S4a,b), suggesting that *PsKMT3* contributes to mycelium growth. The number of sporangia in the mutants was approximately one third that in the WT and CK in 6–12-h samples (Figure S4e). Also, the zoospore number was reduced in the knockout mutants (Figure S4f), but colony morphology, sporangium size, and oospore production were not affected (data not shown). To assess the role of *PsKMT3* under axenic conditions, the effects of stress conditions were evaluated. The *pskmt3* mutants were hypersensitive to hydrogen peroxide ( $H_2O_2$ ) and sodium chloride (NaCl) (Figure S4c,d). In summary, *PsKMT3* is involved in *P. sojae* asexual development and stress responses.

To determine whether *PsKMT3* was required for *P. sojae* virulence, we explored the pathogenicity changes. The 30%–50% reduction in *P. sojae* biomass in *pskmt3* suggested that *PsKMT3* contributes to the virulence of *P. sojae* (Figure 1d,e). The mRNA levels of genes encoding ethylene-responsive element-binding protein (Mazarei et al., 2007), basic  $\beta$ -1,3-endoglucanase (PR2), basic chitinase (PR3) (Saikia et al., 2005), and 1-aminocyclopropane-1-carboxylate synthase 2 (Yang et al., 2019) were significantly up-regulated in *pskmt3*-infected samples compared with WT-infected samples (Figure S5). An enhanced host immune response

and oxidative stress ( $H_2O_2$ ) hypersensitivity in *pskmt3* could explain its reduced pathogenicity.

### 2.3 | H3K36me3 density was reduced in *pskmt3*

To characterize the role of *PsKMT3* in H3K36me3 establishment, we examined methylation in *pskmt3*. The H3K36me3 level in *pskmt3* was significantly reduced to 50% of that in the WT according to western blot analysis using an H3K36me3 antibody (Figure 2a). We next performed chromatin immunoprecipitation followed by sequencing (ChIP-seq) analysis of the WT and *pskmt3* (T89), with two biological replicates (Figure S6c,d). At least 19,000,000 single-end reads were obtained with a mapping ratio of >94% (Table S1). We identified 17,038 and 10,853 methylation peaks in the WT and *pskmt3*, respectively, and *pskmt3* lost approximately one third ( $n = 5,956$ ) of the H3K36me3 peaks and gained 984 peaks (Figure 2b, Tables S2 and S3). We identified 3904 differentially methylated peaks with a false discovery rate (FDR) of <0.05 between the WT and *pskmt3*; the methylation densities of 2370 peaks were reduced, and those of 1534 peaks were increased (Table S4). Overall methylation density was

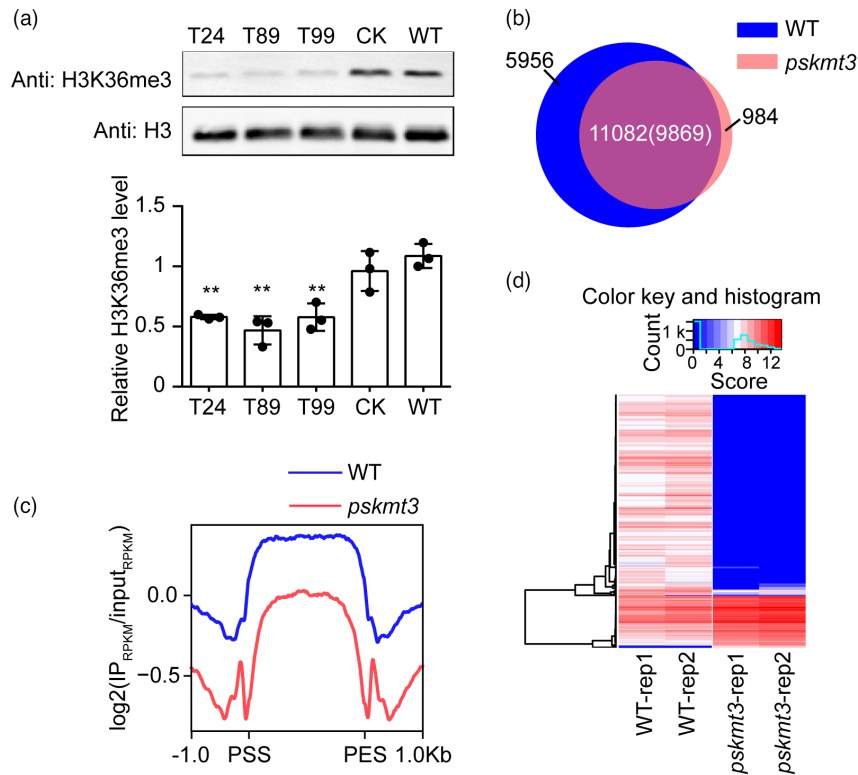


**FIGURE 2** Reduced H3K36me3 density in *pskmt3*. (a) Global H3K36me3 levels in three *pskmt3* knockout mutants (T24, T89, and T99), control (CK), and wild type (WT) as determined by western blot analysis. First lane, H3K36me3 level; second lane, H3 input control level. The relative H3K36me3 level was calculated as the integrated signal density<sub>anti-H3K36me3</sub>/integrated signal density<sub>anti-H3</sub> ratio using ImageJ. The experiments were independently conducted in triplicate. Asterisks indicate a significant difference according to one-way analysis of variance (\*\* $p < 0.01$ ). (b) Venn diagram of H3K36me3 peaks in the WT and *pskmt3*. Blue circle, WT peaks; pink circle, *pskmt3* peaks; numbers, numbers of genes. (c) H3K36me3 levels in differential DiffBind peaks (−1 to +1 kb) in the WT and *pskmt3*. y-axis, H3K36me3 density defined as  $\log_2(\text{RPKM}_{\text{IP}}/\text{RPKM}_{\text{input}})$ . PSS, peak start site; PES, peak end site. (d) Heatmap of the methylation levels in two WT replicates and two *pskmt3* replicates on differential DiffBind peaks. Bar, colour key and histogram of methylation density (reads in peaks) from DiffBind software.

reduced in *pskmt3*, as verified by heatmap analysis (Figure 2c,d). Collectively, our results indicate that PsKMT3 contributes to H3K36me3 in *P. sojae*.

## 2.4 | PsKMT3 regulated the expression of *P. sojae* virulence genes

To dissect the global change of transcriptome and the basis of phenotypic change, we next performed RNA-seq of 3-day-old WT and *pskmt3* mycelium samples (Figure S6a,b). We generated more than 20,000,000 paired-end reads with a mapping ratio of >96% for each biological replicate (Table S5). The expression levels of 13% of genes ( $n = 2610$ ) were affected: 1390 genes were down-regulated and 1220 genes were up-regulated in *pskmt3* compared with the WT (Figure 3a and Table S6). Therefore, knockout of *PsKMT3* markedly affects the *P. sojae* transcriptome. In a Gene Ontology (GO) enrichment analysis (Table S7), the GO items oxidoreductase activity, pathogenesis, extracellular region, and defence response were enriched among the DEGs (Figure 3b). The laccase-encoding gene *PsLCA4* (oxidoreductase activity GO category) was significantly down-regulated (Sheng

et al., 2015) (Figure 3a). A laccase activity assay indicated a 50% reduction in diameter of the 2,2'-azino-di-3-ethylbenzothiazolin e-6-sulfonate (ABTS) oxidation purple area in the three *pskmt3* mutants compared with WT and CK (Figure S7). The hypersensitivity response-inducing gene *SOJ2* was up-regulated in *pskmt3* (Figure 3a). Therefore, the mutant might reduce virulence or enhance host immunity, thereby explaining the reduced pathogenicity of *pskmt3*.

Given that *P. sojae* effectors presumably act as weapons to attack soybean, we checked the expression changes of secreted protein-encoding genes. In *pskmt3*, 374 genes encoding secreted proteins were significantly over-represented among 2610 DEGs ( $\chi^2$  test,  $p = 1.93\text{e-}11$ ) (Figure 3c and Table S7). Next, we evaluated the expression patterns of the genes encoding RxLR, CRN, NLP, YxSL, and elicitor type effectors were compared, using core *P. sojae* genes as the control (Haas et al., 2009; Wang et al., 2018). The majority of differentially expressed RxLR effectors were down-regulated (Figures 3d–f and S8). In total, 42 RxLR genes were differentially expressed, of which 39 were down-regulated (Figure 3e,f). Key virulence effector genes (*Avh23*, *Avh181*, *Avh240*, and *Avh241*) were among the DEGs (Table S6 and Figure S9). Therefore, PsKMT3 is implicated in the regulation of virulence genes in *P. sojae*.

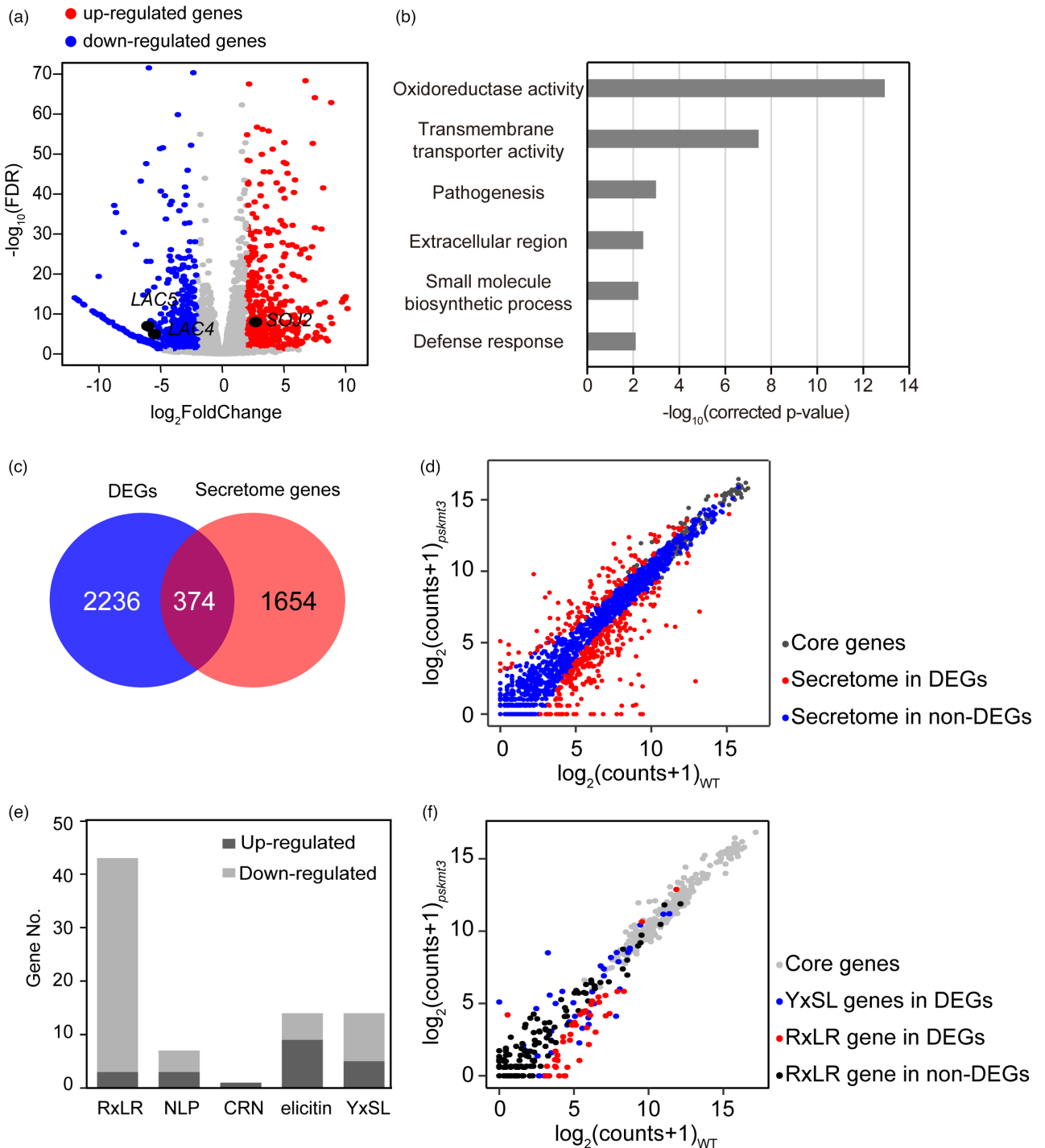


**FIGURE 3** *PsKMT3* regulates *Phytophthora sojae* effector gene expression at the mycelium stage. (a) Volcano plot of RNA-seq data showing differentially expressed genes (DEGs) between the wild type (WT) and *pskmt3*. x-axis,  $\log_2(\text{fold change})$ ; y-axis,  $\log_{10}(\text{FDR})$ . Red dots, genes up-regulated in *pskmt3* compared to the WT ( $\log_2(\text{fold change}) > 1$ ,  $p < 0.05$ ); blue dots, genes down-regulated in *pskmt3* compared to the WT ( $\log_2(\text{fold change}) < -1$ ,  $p < 0.05$ ). (b) GO enrichment of DEGs between the WT and *pskmt3*. x-axis,  $-\log_{10}(\text{corrected } p\text{-value})$ ; y-axis, enriched GO items. (c) Overlap between DEGs and secretome genes. Blue circles, DEGs; red circles, secretome genes; numbers, number of genes. (d) Scatter diagram of the expression levels of secretome genes in the WT and *pskmt3*. x-axis, expression level ( $\log_2(\text{counts}+1)$ ) in the WT; y-axis, expression level ( $\log_2(\text{counts}+1)$ ) in *pskmt3*. Grey dots, core genes; red dots, differentially expressed secretome genes; blue dots, nondifferentially expressed secretome genes. (e) Up- and down-regulated genes in the RxLR, NLP, CRN, elicitin, and YxSL gene families. Grey bar, number of down-regulated genes; dark grey bar, number of up-regulated genes. (f) Expression levels of RxLR, YxSL and core genes in the WT and *pskmt3*. x-axis, WT; y-axis, *pskmt3*. Grey dots, *P. sojae* core genes; blue dots, YxSL genes; red dots, differentially expressed RxLR genes; black dots, other RxLR genes.

## 2.5 | Effector gene transcriptional waves were impaired in *pskmt3* at early infection stages

It is well accepted that effector genes have proper transcriptional waves in infection stages. We performed RNA-seq at 3 and 6 h postinoculation (hpi) to monitor the transcriptional changes in RxLR effector genes between the WT and *pskmt3*. More than 35,000,000 paired-end reads were obtained in each replicate, and the mapping ratios relative to *P. sojae* were 0.13%–0.18% (Table S5). We identified 499 and 489 DEGs at 3 and 6 hpi, respectively, compared with the mycelium in the WT strain (Tables S9 and S10). Among them, we evaluated 314 effector genes that were up-regulated at 3 or 6 hpi in the WT strain to investigate effector gene transcriptional waves ( $\log_2(\text{fold change [FC]}) > 1$ ,  $p < 0.05$ ). We classified these 314 genes based on hierarchical clustering using normalized gene expression data, yielding three clusters (Figure S10). Overall, the genes in cluster 2 were down-regulated in *pskmt3* (Figure S10d,e). Cluster 2 contained eight differentially expressed RxLR genes under the control of PsKMT3 at the mycelium stage. Therefore, these RxLR genes were repressed in *pskmt3* not only in axenic culture but also in planta. Cluster 2 encompassed three RxLR genes, Avh105, Avh292, and Avh137, that suppress BAX-triggered programmed cell death or trigger

*Nicotiana benthamiana* cell death (Wang et al., 2011). This could in part explain the reduced virulence of *pskmt3*.

## 2.6 | H3K36me3 was associated with genome-wide gene activation in *P. sojae*

To investigate the correlation between H3K36me3 and gene expression, we analysed RNA-seq and ChIP-seq data. The genes were divided into 100 groups in descending order based on expression level, and the average transcription and H3K36me3 modification levels were calculated (Figure 4a). A positive association between H3K36me3 and gene expression was observed in both the WT and *pskmt3* ( $R^2_{\text{WT}} = 0.9011$ ,  $p < 2e-16$ ;  $R^2_{\text{pskmt3}} = 0.7883$ ,  $p < 2e-16$ ). The average methylation density of groups 40–81 was lower in *pskmt3* than in the WT. Consistently, these groups had lower gene expression levels (Figure 4a). Therefore, H3K36me3 is associated with highly expressed genes in *P. sojae*, and knockout of *PsKMT3* affected both H3K36me3 and gene expression at the mycelium stage.

To determine whether H3K36me3 deposition was correlated with transcriptome changes, we evaluated the RNA-seq and ChIP-seq FC values. There was a positive correlation

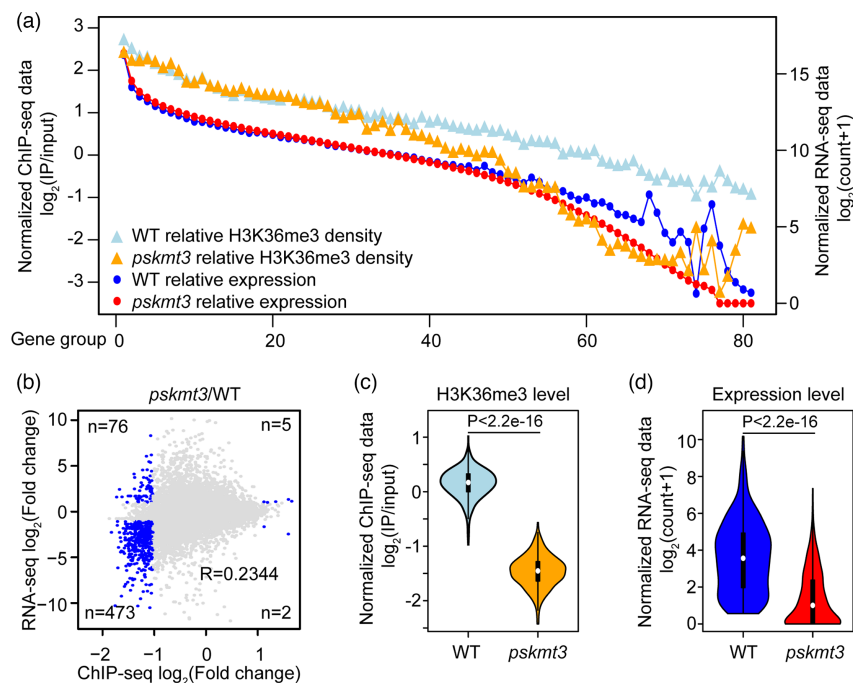


**FIGURE 4** Loss of H3K36me3 contributes to genome-wide gene down-regulation in *pskmt3*. (a) Genome-wide comparison of chromatin immunoprecipitation (ChIP) signals and gene expression in the wild type (WT) and *pskmt3*. A total of 19,196 genes were divided into 100 groups and sorted by descending *pskmt3* expression level; 81 expression groups are shown. x-axis, gene groups; left y-axis, normalized ChIP-seq data ( $\log_2(\text{RPKM}_{\text{IP}}/\text{RPKM}_{\text{input}})$ ); right y-axis, normalized RNA-seq data ( $\log_2(\text{counts}+1)$ ). Light blue triangles, yellow triangles, blue dots, and red dots represent average ChIP signals for *pskmt3* H3K36me3, WT H3K36me3, and expression levels in the WT and *pskmt3*, respectively. (b) ChIP signals and gene expression changes. x-axis, ChIP-seq changes; y-axis, RNA-seq changes. Grey dots, genes with transcriptome and methylation changes of  $-1 < \log_2(\text{fold change}) < 1$ ; blue dots, genes with transcriptome and methylation changes  $|\log_2(\text{fold change})| \geq 1$ . (c) H3K36me3 changes in genes with reduced H3K36me3 peaks; Kolmogorov–Smirnov test. y-axis, normalized ChIP-seq data ( $\log_2(\text{RPKM}_{\text{IP}}/\text{RPKM}_{\text{input}})$ ). (d) Expression changes in genes with reduced H3K36me3 peaks as defined by bedtools with  $>50\%$  overlap. y-axis, normalized RNA-seq data ( $\log_2(\text{counts}+1)$ ); Kolmogorov–Smirnov test.

between H3K36me3 density and gene expression changes ( $R_{\text{pearson}} = 0.2344$ ,  $p < 2e-16$ ) (Figure 4b). The expression and methylation density of 85.07% of genes ( $n = 473$ ) were reduced (Figure 4b), with 556 genes showing twofold changes in both. For 473 genes (Figure 4b), the methylation density ( $p < 2.2e-16$ , Kolmogorov-Smirnov test) and expression ( $p < 2.2e-16$ , Kolmogorov-Smirnov test) (Figure 4c,d) were reduced. Therefore, the H3K36me3 level is correlated with transcriptional activity, and reduced H3K36me3 by *PsKMT3* knockout was associated with down-regulation of gene expression in *pskmt3*.

## 2.7 | Effector gene expression was positively associated with H3K36me3

To elucidate the role of genes whose expression level and methylation density were both reduced, we performed GO analysis. The GO categories 'transmembrane transporter activity' and 'small molecule binding' were enriched (Figure 5a, Table S11), in partial agreement with the DEG GO results (Figure 3b). The GO categories 'obsolete interaction via secreted substance' and 'interspecies interaction between organisms' contained genes encoding effectors (Figure 5a).

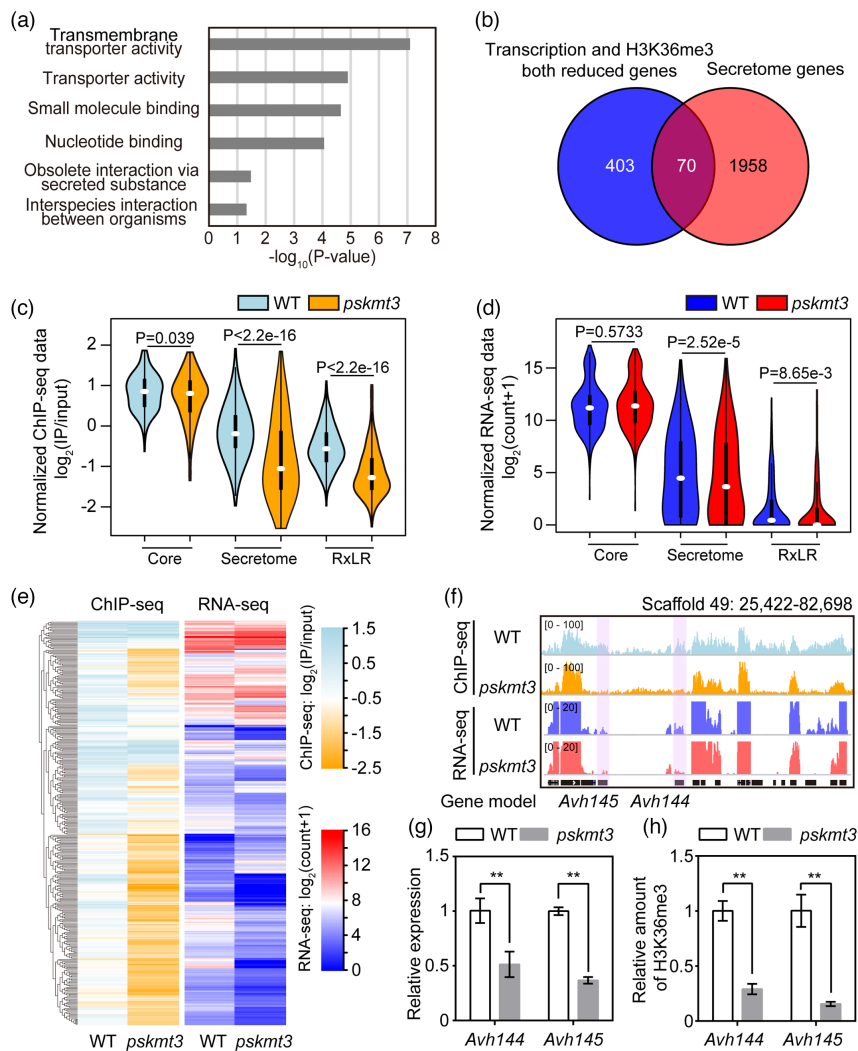


**FIGURE 5** Association between H3K36me3 established by *PsKMT3* and effector gene activation at the mycelium stage. (a) GO enrichment results for genes with reduced expression and H3K36me3 levels ( $\log_2(\text{fold change}) < -1$ ). x-axis,  $-\log_{10}(p\text{-value})$ ; y-axis, enriched GO terms. (b) Overlap of genes with reduced expression and H3K36me3 levels ( $\log_2(\text{fold change}) < -1$ ) and secretome genes. Blue circles, numbers of genes with reduced expression and H3K36me3 levels ( $\log_2(\text{fold change}) < -1$ ); red circles, numbers of secretome genes. (c) H3K36me3 densities in core, secretome, and RxLR genes in the wild type (WT) and *pskmt3*. y-axis, normalized H3K36me3 density values calculated as  $\log_2(\text{RPKM}_{\text{IP}}/\text{RPKM}_{\text{Input}})$ . (d) Expression levels of core, secretome, and RxLR genes in the WT and *pskmt3*. y-axis, normalized expression level calculated as  $\log_2(\text{counts}+1)$ . (e) Heatmap of normalized H3K36me3 density and expression levels of 374 differentially expressed secretome genes. Bar, normalized chromatin immunoprecipitation (ChIP-seq) and RNA-seq values. ChIP-seq data were normalized as  $\log_2(\text{RPKM}_{\text{IP}}/\text{RPKM}_{\text{Input}})$ , and RNA-seq data were normalized as  $\log_2(\text{counts}+1)$ . (f) H3K36me3 and RNA-seq high-throughput sequencing data for *Avh145* and *Avh144*. First and second lanes, ChIP-seq read accumulation; third and fourth lanes, RNA-seq accumulation. (g) Expression levels of *Avh145* and *Avh144* in the WT and *pskmt3* as determined by reverse transcription-quantitative PCR. The expression level in the WT was set to 1. (h) Levels of H3K36me3 in *Avh145* and *Avh144* in the WT and *pskmt3* according to ChIP-quantitative PCR. The H3K36me3 level in the WT was set to 1. Asterisks indicate a significant difference according to Student's *t* test (\*\* $p < 0.01$ ).

Furthermore, a significant number of secretome genes overlapped with genes with reduced expression and methylation density ( $\chi^2$  test,  $p = 0.0008$ ) (Figure 5b). Therefore, PsKMT3-dependent H3K36me3 is associated with effector genes.

To determine whether down-regulation of genes encoding effectors was associated with removal of H3K36me3, we conducted a meta-analysis of the ChIP-seq and RNA-seq data. The ChIP-seq signals in the secretome and RxLR gene groups were lower in *pskmt3* than in the WT, but the methylation levels of core genes were not altered (Figure 5c). We assumed that H3K36me3 established by PsKMT3 has site preference, and methylation of core genes was not PsKMT3-dependent. The expression levels in the secretome and RxLR gene groups were significantly reduced, but those of core genes were unaffected (Figure 5d). Therefore, effector genes were down-regulated by a decreased level of PsKMT3-dependent H3K36me3. The expression and methylation of 374 secretome DEGs were decreased (Figure 5e). Among these genes, we selected eight RxLR genes that were significantly down-regulated in *pskmt3* compared with the WT. CHIP-qPCR validation showed methylation profiles comparable with the ChIP-seq data (Figure S11). We investigated a 57-kb region containing two RxLR genes (*Avh144* and *Avh145*). These two genes showed loss of H3K36me3 peaks and reduced expression, whereas the H3K36me3 and expression levels of neighbouring genes were not altered (Figure 5f–h). Therefore, PsKMT3 regulates effector gene expression at the mycelium stage.

To date, numerous effectors have been identified in *P. sojae*, but the transcriptional regulation of these genes is not well understood. To further verify the hypothesis that H3K36me3 is associated with effector gene regulation, we conducted ChIP-quantitative PCR of H3K36me3 dynamics in four RxLR genes regulated by PsKMT3. In the WT, the H3K36me3 level in *Avh23*, *Avh105*, and *Avh137* was significantly increased during infection, whereas the H3K36me3

level in *Avh181* was lower at the infection stage than at the mycelium stage (Figure 6). Therefore, up-regulation or establishment of H3K36me3 in *Avh23*, *Avh105*, and *Avh137*, but not *Avh181*, was associated with gene induction at the infection stage. The H3K36me3 levels in *Avh23*, *Avh105*, and *Avh137* were markedly decreased at 6 hpi in *pskmt3* compared with the WT (Figure 6). Therefore, PsKMT3 is responsible for H3K36me3 establishment at some RxLR loci during infection. Our findings provide important mechanistic insight into effector gene activation in *P. sojae*.

### 3 | DISCUSSION

Pathogens deploy effector proteins to attack the host; however, the epigenetic regulatory mechanisms of effector gene expression in oomycetes are unclear. Here, we report that the SET domain protein PsKMT3 is involved in regulation of pathogenicity. The H3K36me3 level was decreased genome-wide in the *pskmt3* knockout mutant. Moreover, H3K36me3 was associated with RxLR gene activation. Collectively, our results reveal a role for a SET domain protein in regulating virulence gene expression by modulating histone methylation in *P. sojae*.

PsKMT3 regulated growth, sporulation, zoospore production, and pathogenicity (Figures 1 and S4), as in other microbes. KMT3 family mutants show defective asexual growth and pathogenicity in the rice blast fungus *Fusarium verticillioides* and in *E. festucae* (Gu et al., 2017; Lukito et al., 2020; Pham et al., 2015). H3K36me3 plays important roles in filamentous plant pathogens. In the *pskmt3* mutant, the host immune response was enhanced, including up-regulation of the ethylene-responsive gene *PR2* and of the ethylene- and jasmonic acid-responsive gene *PR3* (Figure S5). Therefore, defective infection is unlikely due to the slow growth of *pskmt3*.

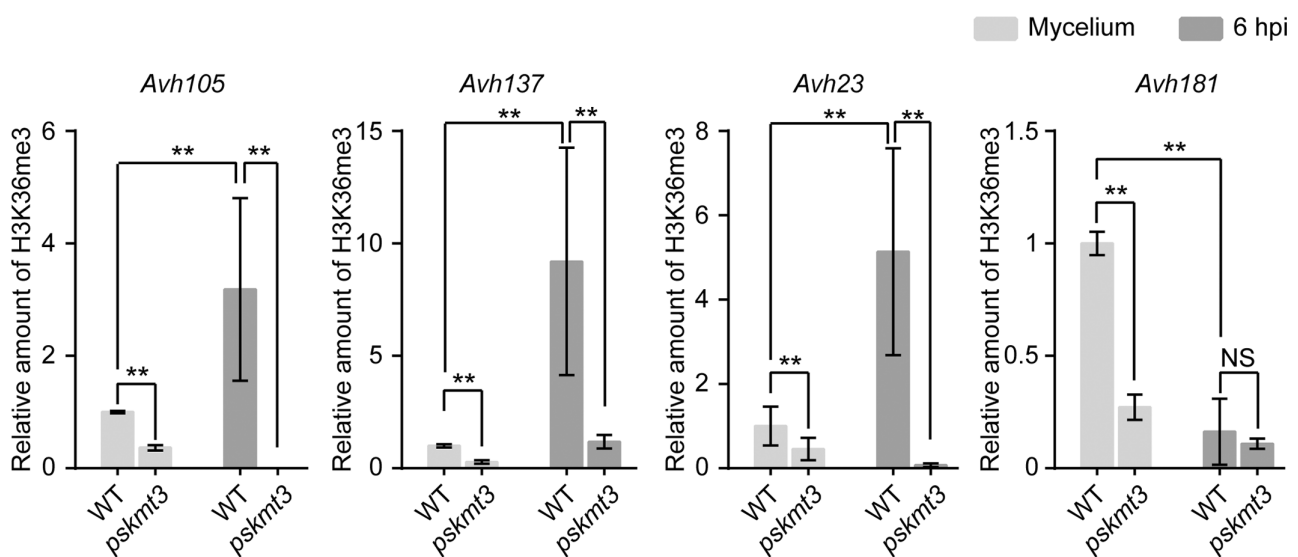


FIGURE 6 H3K36me3 dynamics in four RxLR genes at the mycelium stage and 6 h postinoculation. H3K36me3 levels in *Avh105*, *Avh137*, *Avh23*, and *Avh181* in the wild type (WT) and *pskmt3* during axenic growth and infection. The H3K36me3 level in the WT at the mycelium stage was set to 1. Asterisks indicate a significant difference according to Student's *t* test (\*\* $p < 0.01$ ).

In the *pskmt3* mutant, gene expression may be affected, causing phenotypic defects. The transcription factor (TF)-encoding genes *PsMYB1* and *PsMAD1*, which are related to zoospore release and pathogenicity (Lin et al., 2018; Zhang et al., 2012), were differentially expressed in the *pskmt3* mutant compared with the WT (Table S6). Also, of 462 genes, 109 were involved in small molecule metabolic processes (Table S7). We hypothesize that dysregulation of genes related to small molecule metabolic processes influences *P. sojae* development. We conclude that PsKMT3 has potential as a fungicide target because of its important roles in development and virulence.

The mechanisms of H3K36me3 establishment have been reported in several model species (Bhattacharya et al., 2021; Kizer et al., 2005; Liu et al., 2019; Wagner & Carpenter, 2012), but they are unclear in *P. sojae*. The SRI domain contributes to H3K36me3 deposition by directly interacting with RNA polymerase II subunit B1, the large subunit of RNA polymerase II (Hyun et al., 2017; Kizer et al., 2005). Interestingly, no SRI domain was found in *P. sojae* (Figure S1). Western blot analysis indicated retention of almost 50% of H3K36me3 in *pskmt3*; consistently, 9869 H3K36me3 peaks detected by ChIP-seq were present in *pskmt3* T89 (Figure 2). Therefore, H3K36me3 was not completely lost after knockout of *PsKMT3*. Two SET2 homologues are present in filamentous fungi. Double knockout of the two homologues led to loss of H3K36me2/me3, whereas >20% of H3K36me3 was retained in a single deletion mutant (Gu et al., 2017; Janevska et al., 2018). Other KMT3 family members might be involved in H3K36me3 establishment in *P. sojae* (Figure S1a).

Effector regulation in filamentous microbes, including TFs, chromosome-based control, and effector epistasis, has been reviewed (Tan & Oliver, 2017). Our findings suggest H3K36me3 mediates RxLR effector gene activation. In the grass-symbiotic fungus *E. festucae*, effector genes are significantly over-represented among DEGs regulated by Set2-mediated H3K36me (Lukito et al., 2020). Moreover, in the parasite *Plasmodium falciparum*, several multicopy virulence gene families (var, rifin, and stevor) are repressed in a PfSETvs-dependent H3K36me3 manner (Jiang et al., 2013). In this study, numerous effectors were differentially up- and down-regulated in *pskmt3* (Figure 3). This resembles the effector gene expression pattern in *E. festucae* (Lukito et al., 2020). H3K36me3 was associated with RxLR gene activation at the mycelium stage. Indeed, the H3K36me3 patterns of the eight tested RxLR genes were consistent with the ChIP-seq results (Figures 5 and S11). *Avh105* and *Avh137* were up-regulated upon infection by the WT and were strongly down-regulated to an almost silent state in *pskmt3* (Figures S9 and S10). The H3K36me3 levels at the *Avh105* and *Avh137* loci were significantly increased at the infection stage. The methylation level was reduced at both stages, suggesting that the H3K36me3 level at these two loci is regulated in a PsKMT3-dependent manner. By comparison, methylation of *Avh23* and *Avh181* is neither sufficient nor required for gene up-regulation. We hypothesize that this type of effector gene is controlled by other mechanisms. Effector genes in *Leptosphaeria maculans* are controlled by histone marks and TFs

(Clairet et al., 2021). We investigated potential TF-binding sites or cis-regulatory elements in the 39 down-regulated RxLR genes by motif searching across 1-kb promoter regions, yielding two highly reliable motifs: motif 1 (AACCGACTGVWGC) and motif 2 (CAAACKTGAGCVATD). These two motifs were similar to 12 footprint-supported cis-regulatory elements (Zhang et al., 2022) (Table S12). Therefore, H3K36me3 formation at RxLR loci might be caused by TFs. Our results also suggest that H3K36me3 is directly and indirectly involved in the regulation of effector gene expression.

Effector expression waves have been reported in plant pathogens (Dong et al., 2015; Gay et al., 2021; Gervais et al., 2017; Haueisen et al., 2019; Palma-Guerrero et al., 2016; Rocher et al., 2022; Wang et al., 2011). However, the regulation of large-scale effector expression waves is unclear. Fine tuning of virulence gene expression affects pathogen virulence, and effector-wave functions have been investigated (Gervais et al., 2017; Ochola et al., 2020; Wang et al., 2011). In this study, we found dysregulation of effector gene expression waves among the mycelium, 3 hpi, and 6 hpi stages in *pskmt3* (Figure S11). Questions regarding effector gene wave regulation, cross-talk, and feedback between histone modifications and TFs warrant further investigation. Our findings emphasize the importance of effector gene regulation in the development of novel management strategies for crop diseases.

## 4 | EXPERIMENTAL PROCEDURES

### 4.1 | Strain culturing, *P. sojae* transformation, and soybean cultivation

*P. sojae* strain P6497, which served as the WT, was used in the study. It was routinely maintained on 10% V8 medium at 25°C in the dark. *P. sojae* transformation was performed as previously reported (Fang & Tyler, 2016). The susceptible soybean cultivar Hefeng47 and Williams were provided after growing at 25°C (16 h) and 22°C (8 h) in the dark for 4 days.

### 4.2 | Phylogenetic analysis and domain organization analysis

ScSET2(NP\_012367.2) and NcSET2(XP\_957740.1) were set as queries against 10 oomycetes with e-values <10<sup>-20</sup>. Besides, published H3K36me3 methyltransferases NSD1, NSD2, NSD3, Ash1L, DmSet2, DmMES4, and DmAsh1 were included. The phylogenetic tree was constructed by MEGA X using the maximum-likelihood method.

The domain organization information was searched using the NCBI Conserved Domain database by batch CD-search with default parameters. The phylogenetic tree was constructed and domain organization analysis was conducted by TBtools with

protein fasta sequence and domain organization information (Chen et al., 2020).

### 4.3 | Growth, sporangium and zoospore production

All strains were grown on 10% V8 medium at 25°C in the dark. Colony diameters were measured during a period of 5 days and the average growth rate was calculated.

To compare sporangium production, six mycelial plugs of different strains were incubated on 10% V8 liquid medium for 3 days in the dark. The mycelium was then rinsed twice with double-deionized water. The samples were collected at 6, 9, and 12 h after rinsing, and then each sample was gently mixed by a blender. One hundred microlitres of each mixture was taken and sporangia were counted under a microscope. All assays were repeated three times.

To compare zoospore production, three mycelial plugs of different strains were incubated on 10% V8 medium for 3 days in the dark. The plates were rinsed twice with double-deionized water every 30 min. Zoospores were observed under a microscope and the number of zoospores was recorded (0 min). Two microlitres of each sample was taken every 30 min for 2.5 h and zoospores were counted under a microscope. All assays were repeated three times.

### 4.4 | Virulence assays

Zoospores were released by rinsing the V8 plates with sterile water. Then 100 zoospores were dropped on soybean Hefeng47 hypocotyls, and the infected samples were kept at 25°C and 80% relative humidity in the dark. Pictures were captured at 2 days postinoculation to analyse pathogenicity. The DNA of infected samples was extracted using a TIANGEN DNA secure kit. Relative biomass was quantified by quantitative PCR (qPCR) as previously reported (Qiu et al., 2022).

### 4.5 | Protein extraction, western blot, and protein quantification

Three-day-old *P. sojae* mycelia collected from liquid cultures were ground in liquid nitrogen. Next, 800 µl lysis buffer (1% SDS in Tris-EDTA buffer) was added to 100 mg of pulverized mycelium powder. Lysates were mixed by vortexing for 30 min at 4°C. Supernatants of protein samples were mixed with loading buffer (Beyotime, P0015) and denatured at 95°C for 10 min. Anti-H3K36me3 (abcam; ab9050) and anti-H3 (abcam; ab1791) were used as primary antibodies, and goat anti-rabbit IRDye 800CW (Odyssey, no. 926-32211; Li-Cor) was used as a secondary antibody. The signals were recorded by an Odyssey laser imaging system (Li-Cor company) and quantified using ImageJ. The H3K36me3 level was calculated as  $\text{signal}_{\text{H3K36me3}}/\text{signal}_{\text{H3}}$ , and H3K36me3 levels were compared with the levels in WT.

## 4.6 | Native ChIP-seq, ChIP-qPCR, and RNA-seq

Mycelium stage samples for native ChIP-seq and RNA-seq were collected from liquid cultures of 3-day-old WT and *pskmt3* T89. For 3 hpi and 6 hpi samples, zoospores were released by rinsing the V8 plates with sterile water. Then 100 zoospores were dropped on soybean Williams hypocotyls, and the infected samples were kept at 25°C and 80% relative humidity in the dark. Infected samples were collected 3 h and 6 h after incubation for ChIP-qPCR and RNA-seq analysis. The samples were dried by filter paper and ground with mortar and pestle in liquid nitrogen. Native ChIP experiments were performed as previously described (Wang et al., 2020). Briefly, nuclei were extracted and then digested by micrococcal nuclease (New England BioLabs). The size of digested chromatin was around 150–300 bp and 300–600 bp for ChIP-seq and ChIP-qPCR, respectively. Two replicates were carried out for ChIP-seq and RNA-seq. Input and immunoprecipitated DNA samples were sequenced by BGI Company by 50-bp single-end sequencing. RNA samples were extracted using the Omega Total RNA Kit I. RNA-seq libraries were prepared by BGI Company and sequenced using a BGISEQ-500 platform. ChIP-qPCR experiments were carried out three times with similar results.

## 4.7 | High-throughput sequencing data analysis

Clean ChIP-seq reads were mapped to the *P. sojae* reference genome v. 1.1 using Bowtie 2 with max mismatch = 1 (v. 2.3.5.1) (Langmead & Salzberg, 2012). The aligned bam files were sorted and indexed by samtools in default mode (v. 1.7) (Li et al., 2009). Principal component analysis (PCA) plots were drawn and heatmap clustering of ChIP-seq data was performed using “plotPCA” and “plotCorrelation” in deepTools, respectively (Ramírez et al., 2014). ChIP-seq peaks were defined by MACS2 employing a “-broad” model (Gaspar, 2018). Peak overlaps were analysed by “intersectBed” in bedtools (Quinlan & Hall, 2010). DiffBind was used to define differential methylation peaks (Stark & Brown, 2023). The H3K36me3 heatmap of differential methylation peaks in Figure 2d was produced by DiffBind. The ChIP signals were calculated as  $\log_2(\text{RPKM}_{\text{ChIP}}/\text{RPKM}_{\text{Input}})$  by DeepTools (v. 3.4.3) “bamCompare” using a bam file of IP and input RPKM values as input. ChIP-seq data were visualized using the TBtools-Graphics-Heatmap Illustrator-Heatmap function (Figure 5e) and Integrative Genome Viewer (v. 2.8.0) (<https://software.broadinstitute.org/software/igv/>) (Figure 5f). ChIP-seq FC values for each gene were defined by read count changes in the IP group and calculated using DESeq2 (Love et al., 2014).

Clean RNA-seq reads were aligned to the genomes using HISAT2 (v. 2.1.0) (Kim et al., 2015), and the aligned bam files were sorted and indexed by samtools in default mode (v. 1.9). The bam file was converted to tdf files for visualization using Integrative Genome Viewer. Gene expression data were calculated by StringTie v. 2.1.2 (Pertea et al., 2015), and gene expression data

of Figure S7 were from a published dataset (Ye et al., 2011). PCA plots were drawn and heatmap clustering of RNA-seq data was performed using “plotPCA” and “plotCorrelation” in deepTools. Expression patterns were clustered by the TBtools-Graphics-Heatmap Illustrator-Heatmap function (Chen et al., 2020). The heatmap was based on the complete-linkage method, and the gene clusters were based on hierarchical clustering. CRN, NLP, YxSL, elicitor, RxLR, and secretome genes in Figures 2d and S6 were compared by ggplot2. GO enrichment was analysed by the TBtools-GO&KEGG-Gene ontology-GO enrichment function (Chen et al., 2020). RNA-seq FC values for each gene were defined by read count changes using DESeq2. The secretome genes were identified with the SignalP v. 5.0 online tool using *P. sojae* v. 1.1 protein sequences (Almagro Armenteros et al., 2019).

#### 4.8 | Motif searching

Motif searching was performed using the MEME suite (Bailey et al., 2015) STREME using 1-kb upstream sequences of 39 RxLR genes as input. The 1-kb upstream sequences of all RxLR genes were used as control sequences. Motifs with a length of 8–15 bp were selected. TomTom was used to compare two selected motifs against published motifs. The significance threshold was  $e^{-10}$ .

#### ACKNOWLEDGEMENTS

This work was supported by grants from the Chinese National Key Research and Development Program (2022YFC2601000) to S.D., the National Natural Science Foundation of China (NSFC) (32100158), the China Postdoctoral Science Foundation (2020M681641), and the Fundamental Research Funds for the Central Universities (KYQN2022059) to H.C. This work was also supported by NSFC (31721004) to Y.W. We are grateful to the Bioinformatics Center at Nanjing Agricultural University for support of the bioinformatics analysis. We thank the NJAU oomycete research group for valuable discussions. [Correction added on 14 February 2023, after first online publication: the Acknowledgement section has been updated in this version.]

#### CONFLICT OF INTEREST

The authors have no conflict of interest.

#### DATA AVAILABILITY STATEMENT

The datasets supporting the conclusions of this article are available in the Gene Expression Omnibus database of NCBI at <https://www.ncbi.nlm.nih.gov/geo/>. ChIP-seq datasets and RNA-seq datasets are deposited with GEO numbers GSE205359 and GSE205360, respectively.

#### ORCID

Han Chen  <https://orcid.org/0000-0003-1396-4514>

Wenwu Ye  <https://orcid.org/0000-0001-7347-8935>

Yuanchao Wang  <https://orcid.org/0000-0001-5803-5343>

Suomeng Dong  <https://orcid.org/0000-0002-9623-6776>

#### REFERENCES

- Allis, C.D., Berger, S.L., Cote, J., Dent, S., Jenuwien, T., Kouzarides, T. et al. (2007) New nomenclature for chromatin-modifying enzymes. *Cell*, 131, 633–636.
- Almagro Armenteros, J.J., Tsirigos, K.D., Sønderby, C.K., Petersen, T.N., Winther, O., Brunak, S. et al. (2019) SignalP 5.0 improves signal peptide predictions using deep neural networks. *Nature Biotechnology*, 37, 420–423.
- Bailey, T.L., Johnson, J., Grant, C.E. & Noble, W.S. (2015) The MEME suite. *Nucleic Acids Research*, 43, W39–W49.
- Bhattacharya, S., Levy, M.J., Zhang, N., Li, H., Florens, L., Washburn, M.P. et al. (2021) The methyltransferase SETD2 couples transcription and splicing by engaging mRNA processing factors through its SHI domain. *Nature Communications*, 12, 1443.
- Bialas, A., Zess, E.K., De La Concepcion, J.C., Franceschetti, M., Pennington, H.G., Yoshida, K. et al. (2018) Lessons in effector and NLR biology of plant–microbe systems. *Molecular Plant–Microbe Interactions*, 31, 34–45.
- Chen, C.J., Chen, H., Zhang, Y., Thomas, H.R., Frank, M.H., He, Y.H. et al. (2020) TBtools: an integrative toolkit developed for interactive analyses of big biological data. *Molecular Plant*, 13, 1194–1202.
- Chen, H., Raffaele, S. & Dong, S.M. (2021) Silent control: microbial plant pathogens evade host immunity without coding sequence changes. *FEMS Microbiology Reviews*, 45, fuab002.
- Chujo, T. & Scott, B. (2014) Histone H3K9 and H3K27 methylation regulates fungal alkaloid biosynthesis in a fungal endophyte–plant symbiosis. *Molecular Microbiology*, 92, 413–434.
- Clairet, C., Gay, E.J., Porquier, A., Blaise, F., Marais, C.L., Balesdent, M.H. et al. (2021) Regulation of effector gene expression as concerted waves in *Leptosphaeria maculans*: a two-players game. *bioRxiv*, <https://doi.org/10.1101/2021.12.15.472773> [preprint].
- Collemare, J. & Seidl, M.F. (2019) Chromatin-dependent regulation of secondary metabolite biosynthesis in fungi: is the picture complete? *FEMS Microbiology Reviews*, 43, 591–607.
- Dillon, S.C., Zhang, X., Trievel, R.C. & Cheng, X. (2005) The SET-domain protein superfamily: protein lysine methyltransferases. *Genome Biology*, 6, 227.
- Dong, Y., Li, Y., Zhao, M., Jing, M., Liu, X., Liu, M. et al. (2015) Global genome and transcriptome analyses of *Magnaporthe oryzae* epidemic isolate 98-06 uncover novel effectors and pathogenicity-related genes, revealing gene gain and loss dynamics in genome evolution. *PLoS Pathogens*, 11, e1004801.
- Fang, Y. & Tyler, B.M. (2016) Efficient disruption and replacement of an effector gene in the oomycete *Phytophthora sojae* using CRISPR/Cas9. *Molecular Plant Pathology*, 17, 127–139.
- Freitag, M. (2017) Histone methylation by SET domain proteins in fungi. *Annual Review of Microbiology*, 71, 413–439.
- Gaspar, J.M. (2018) Improved peak-calling with MACS2. *bioRxiv*, <https://doi.org/10.1101/496521> [preprint].
- Gay, E.J., Soyer, J.L., Lapalu, N., Linglin, J., Fudal, I., DA Silva, C. et al. (2021) Large-scale transcriptomics to dissect 2 years of the life of a fungal phytopathogen interacting with its host plant. *BMC Biology*, 19, 55.
- Gervais, J., Plissonneau, C., Linglin, J., Meyer, M., Labadie, K., Cruaud, C. et al. (2017) Different waves of effector genes with contrasted genomic location are expressed by *Leptosphaeria maculans* during cotyledon and stem colonization of oilseed rape. *Molecular Plant Pathology*, 18, 1113–1126.
- Gu, Q., Wang, Z.Z., Sun, X., Ji, T.T., Huang, H., Yang, Y. et al. (2017) FvSet2 regulates fungal growth, pathogenicity, and secondary metabolism in *Fusarium verticillioides*. *Fungal Genetics and Biology*, 107, 24–30.
- Haas, B.J., Kamoun, S., Zody, M.C., Jiang, R.H., Handsaker, R.E., Cano, L.M., et al. (2009) Genome sequence and analysis of the Irish potato famine pathogen *Phytophthora infestans*. *Nature*, 461, 393–398.

- Hauelsen, J., Moller, M., Eschenbrenner, C.J., Grandaubert, J., Seybold, H., Adamiak, H. et al. (2019) Highly flexible infection programs in a specialized wheat pathogen. *Ecology and Evolution*, 9, 275–294.
- Hyun, K., Jeon, J., Park, K. & Kim, J. (2017) Writing, erasing and reading histone lysine methylations. *Experimental & Molecular Medicine*, 49, e324.
- Janevska, S., Baumann, L., Sieber, C.M.K., Münsterkötter, M., Ulrich, J., Kämper, J. et al. (2018) Elucidation of the two H3K36me3 histone Methyltransferases Set2 and Ash1 in *Fusarium fujikuroi* unravels their different chromosomal targets and a major impact of Ash1 on genome stability. *Genetics*, 208, 153–171.
- Jiang, R.H. & Tyler, B.M. (2012) Mechanisms and evolution of virulence in oomycetes. *Annual Review of Phytopathology*, 50, 295–318.
- Jiang, L., Mu, J., Zhang, Q., Ni, T., Srinivasan, P., Rayavara, K. et al. (2013) PfSETvs methylation of histone H3K36 represses virulence genes in *Plasmodium falciparum*. *Nature*, 499, 223–227.
- Jones, J.D.G. & Dangl, J.L. (2006) The plant immune system. *Nature*, 444, 323–329.
- Kim, S., Kim, H., Fong, N., Erickson, B. & Bentley, D.L. (2011) Pre-mRNA splicing is a determinant of histone H3K36 methylation. *Proceedings of the National Academy of Sciences of the United States of America*, 108, 13564–13569.
- Kim, D., Langmead, B. & Salzberg, S.L. (2015) HISAT: a fast spliced aligner with low memory requirements. *Nature Methods*, 12, 357–360.
- Kizer, K.O., Phatnani, H.P., Shibata, Y., Hall, H., Greenleaf, A.L. & Strahl, B.D. (2005) A novel domain in Set2 mediates RNA polymerase II interaction and couples histone H3 K36 methylation with transcript elongation. *Molecular and Cellular Biology*, 25, 3305–3316.
- Kramer, H.M., Seidl, M.F., Thomma, B.P.H.J., Cook, D.E., Fudal, I. & Di Pietro, A. (2022) Local rather than global H3K27me3 dynamics are associated with differential gene expression in *Verticillium dahliae*. *mBio*, 13, e0356621.
- Landry, J., Sutton, A., Hesman, T., Min, J., Xu, R.M., Johnston, M. et al. (2003) Set2-catalyzed methylation of histone H3 represses basal expression of GAL4 in *Saccharomyces cerevisiae*. *Molecular and Cellular Biology*, 23, 5972–5978.
- Langmead, B. & Salzberg, S.L. (2012) Fast gapped-read alignment with bowtie 2. *Nature Methods*, 9, 357–359.
- Li, H., Handsaker, B., Wysoker, A., Fennell, T., Ruan, J., Homer, N. et al. (2009) The sequence alignment/map format and SAMtools. *Bioinformatics*, 25, 2078–2079.
- Lin, L., Ye, W., Wu, J., Xuan, M., Li, Y., Gao, J. et al. (2018) The MADS-box transcription factor PsMAD1 is involved in zoosporogenesis and pathogenesis of *Phytophthora sojae*. *Frontiers in Microbiology*, 9, 2259.
- Liu, B., Liu, Y., Wang, B., Luo, Q., Shi, J., Gan, J. et al. (2019) The transcription factor OsSUF4 interacts with SDG725 in promoting H3K36me3 establishment. *Nature Communications*, 10, 2999.
- Love, M.I., Huber, W. & Anders, S. (2014) Moderated estimation of fold change and dispersion for RNA-seq data with DESeq2. *Genome Biology*, 15, 550.
- Lukito, Y., Lee, K., Noorifar, N., Green, K.A., Winter, D.J., Ram, A. et al. (2020) Regulation of host-infection ability in the grass-symbiotic fungus *Epichloë festucae* by histone H3K9 and H3K36 methyltransferases. *Environmental Microbiology*, 23, 2116–2131.
- Mazarei, M., Elling, A.A., Maier, T.R., Puthoff, D.P. & Baum, T.J. (2007) GmEREBP1 is a transcription factor activating defense genes in soybean and *Arabidopsis*. *Molecular Plant-Microbe Interactions*, 20, 107–119.
- Meile, L., Peter, J., Puccetti, G., Alassimone, J., McDonald, B.A. & Sánchez-Vallet, A. (2020) Chromatin dynamics contribute to the spatiotemporal expression pattern of virulence genes in a fungal plant pathogen. *mBio*, 11, e02343-20.
- Ngou, B.P.M., Ding, P. & Jones, J.D.G. (2022) Thirty years of resistance: zig-zag through the plant immune system. *The Plant Cell*, 34, 1447–1478.
- Ochola, S., Huang, J., Ali, H., Shu, H., Shen, D., Qiu, M. et al. (2020) Editing of an effector gene promoter sequence impacts plant-*Phytophthora* interaction. *Journal of Integrative Plant Biology*, 62, 378–392.
- Palma-Guerrero, J., Torriani, S.F., Zala, M., Carter, D., Courbot, M., Rudd, J.J. et al. (2016) Comparative transcriptomic analyses of *Zymoseptoria tritici* strains show complex lifestyle transitions and intraspecific variability in transcription profiles. *Molecular Plant Pathology*, 17, 845–859.
- Perteua, M., Perteua, G.M., Antonescu, C.M., Chang, T.C., Mendell, J.T. & Salzberg, S.L. (2015) StringTie enables improved reconstruction of a transcriptome from RNA-seq reads. *Nature Biotechnology*, 33, 290–295.
- Petre, B., Lorrain, C., Stukenbrock, E.H. & Duplessis, S. (2020) Host-specialized transcriptome of plant-associated organisms. *Current Opinion in Plant Biology*, 56, 81–88.
- Pham, K.T., Inoue, Y., Vu, B.V., Nguyen, H.H., Nakayashiki, T., Ikeda, K. et al. (2015) MoSET1 (histone H3K4 Methyltransferase in *Magnaporthe oryzae*) regulates global gene expression during infection-related morphogenesis. *PLoS Genetics*, 11, e1005385.
- Qiu, X.F., Kong, L., Chen, H., Lin, Y.C., Tu, S.Q., Wang, L. et al. (2022) The *Phytophthora sojae* nuclear effector PsAvh110 targets a host transcriptional complex to modulate plant immunity. *The Plant Cell*, 35, 574–597.
- Quinlan, A.R. & Hall, I.M.J.B. (2010) BEDTools: a flexible suite of utilities for comparing genomic features. *Bioinformatics*, 26, 841–842.
- Ramírez, F., Dündar, F., Diehl, S., GRüning, B.A. & Manke, T. (2014) deepTools: a flexible platform for exploring deep-sequencing data. *Nucleic Acids Research*, 42, 187–191.
- Rando, O.J. & Chang, H.Y. (2009) Genome-wide views of chromatin structure. *Annual Review of Biochemistry*, 78, 245–271.
- Rechtsteiner, A., Ercan, S., Takasaki, T., Phippen, T.M., Egelhofer, T.A., Wang, W. et al. (2010) The histone H3K36 methyltransferase MES-4 acts epigenetically to transmit the memory of germline gene expression to progeny. *PLoS Genetics*, 6, e1001091.
- Rocher, F., Alouane, T., Philippe, G., Martin, M.-L., Label, P., Langin, T. et al. (2022) *Fusarium graminearum* infection strategy in wheat involves a highly conserved genetic program that controls the expression of a core effectome. *International Journal of Molecular Sciences*, 23, 1914.
- Saikia, R., Singh, B.P., Kumar, R. & Arora, D.K. (2005) Detection of pathogenesis-related proteins – chitinase and  $\beta$ -1, 3-glucanase in induced chickpea. *Current Science*, 89, 659–663.
- Sanchez, R. & Zhou, M.-M. (2011) The PHD finger: a versatile epigenome reader. *Trends in Biochemical Sciences*, 36, 364–372.
- Sánchez-Vallet, A. (2018) The genome biology of effector gene evolution in filamentous plant pathogens. *Annual Review of Phytopathology*, 56, 21–40.
- Sheng, Y., Wang, Y., Meijer, H.J., Yang, X., Hua, C., Ye, W. et al. (2015) The heat shock transcription factor PsHSF1 of *Phytophthora sojae* is required for oxidative stress tolerance and detoxifying the plant oxidative burst. *Environmental Microbiology*, 17, 1351–1364.
- Shi, X., Kachirskaia, I., Walter, K.L., Kuo, J.-H.A., Lake, A., Davrazou, F. et al. (2007) Proteome-wide analysis in *Saccharomyces cerevisiae* identifies several PHD fingers as novel direct and selective binding modules of histone H3 methylated at either lysine 4 or lysine 36. *Journal of Biological Chemistry*, 282, 2450–2455.
- Soyer, J.L., EL Ghalid, M., Glaser, N., Ollivier, B., Linglin, J., Grandaubert, J. et al. (2014) Epigenetic control of effector gene expression in the plant pathogenic fungus *Leptosphaeria maculans*. *PLoS Genetics*, 10, e1004227.
- Stark, R.A. & Brown, G. (2023) DiffBind: differential binding analysis of ChIP-Seq peak data [Online]. Available: <http://bioconductor.org/packages/release/bioc/vignettes/DiffBind/inst/doc/DiffBind.pdf> [Accessed 26th January 2023].
- Strahl, B.D., Grant, P.A., Briggs, S.D., Sun, Z.W., Bone, J.R., Caldwell, J.A. et al. (2002) Set2 is a nucleosomal histone H3-selective

- methyltransferase that mediates transcriptional repression. *Molecular and Cellular Biology*, 22, 1298–1306.
- Sun, Z., Zhang, Y., Jia, J., Fang, Y., Tang, Y., Wu, H. et al. (2020) H3K36me3, message from chromatin to DNA damage repair. *Cell & Bioscience*, 10, 9.
- Tan, K.C. & Oliver, R.P. (2017) Regulation of proteinaceous effector expression in phytopathogenic fungi. *PLoS Pathogens*, 13, e1006241.
- Tyler, B.M. (2007) *Phytophthora sojae*: root rot pathogen of soybean and model oomycete. *Molecular Plant Pathology*, 8, 1–8.
- Wagner, E.J. & Carpenter, P.B. (2012) Understanding the language of Lys36 methylation at histone H3. *Nature Reviews Molecular Cell Biology*, 13, 115–126.
- Wang, L.Y., Chen, H., Li, J.J., Shu, H.D., Zhang, X.X., Wang, Y.C. et al. (2020) Effector gene silencing mediated by histone methylation underpins host adaptation in an oomycete plant pathogen. *Nucleic Acids Research*, 48, 1790–1799.
- Wang, Q.Q., Han, C.Z., Ferreira, A.O., Yu, X.L., Ye, W.W., Tripathy, S. et al. (2011) Transcriptional programming and functional interactions within the *Phytophthora sojae* RXLR effector repertoire. *The Plant Cell*, 23, 2064–2086.
- Wang, Y. & Wang, Y. (2018) *Phytophthora sojae* effectors orchestrate warfare with host immunity. *Current Opinion in Microbiology*, 46, 7–13.
- Wang, Y., Ye, W. & Wang, Y. (2018) Genome-wide identification of long non-coding RNAs suggests a potential association with effector gene transcription in *Phytophthora sojae*. *Molecular Plant Pathology*, 19, 2177–2186.
- Wrather, J.A. & Koening, S.R. (2006) Estimates of disease effects on soybean yields in the United States 2003 to 2005. *Journal of Nematology*, 38, 173–180.
- Yang, B., Wang, Y., Guo, B., Jing, M., Zhou, H., Li, Y. et al. (2019) The *Phytophthora sojae* RXLR effector Avh238 destabilizes soybean Type2 GmACSs to suppress ethylene biosynthesis and promote infection. *The New Phytologist*, 222, 425–437.
- Ye, W., Wang, X., Tao, K., Lu, Y., Dai, T., Dong, S. et al. (2011) Digital gene expression profiling of the *Phytophthora sojae* transcriptome. *Molecular Plant-Microbe Interactions*, 24, 1530–1539.
- Zhang, M., Lu, J., Tao, K., Ye, W.W., Li, A.N., Liu, X.Y. et al. (2012) A Myb transcription factor of *Phytophthora sojae*, regulated by MAP kinase PsSAK1, is required for zoospore development. *PLoS One*, 7, e40246.
- Zhang, W., Huang, J. & Cook, D.E. (2021) Histone modification dynamics at H3K27 are associated with altered transcription of in planta induced genes in *Magnaporthe oryzae*. *PLoS Genetics*, 17, e1009376.
- Zhang, Z., Lin, L., Chen, H., Ye, W., Dong, S., Zheng, X. et al. (2022) ATAC-Seq reveals the landscape of open chromatin and cis-regulatory elements in the *Phytophthora sojae* genome. *Molecular Plant-Microbe Interactions*, 35, 301–310.

## SUPPORTING INFORMATION

Additional supporting information can be found online in the Supporting Information section at the end of this article.

**How to cite this article:** Chen, H., Fang, Y., Song, W., Shu, H., Li, X., Ye, W. et al. (2023) The SET domain protein PsKMT3 regulates histone H3K36 trimethylation and modulates effector gene expression in the soybean pathogen *Phytophthora sojae*. *Molecular Plant Pathology*, 24, 346–358. Available from: <https://doi.org/10.1111/mpp.13301>